

Article

Graphite Nanoplatelets Nanostructured Films as Multifunctional Protective Layer in Kevlar/Nomex Sandwich Composites

Fabrizia Cilento ¹, Barbara Palmieri ^{1,*}, Giovangiuseppe Giusto ^{2,3}, Ruggiero Volponi ², Giovanni Bruno ², Carmine Carandente Tartaglia ², Cinzia Toscano ², Michele Giordano ¹ and Alfonso Martone ^{1,3,*}

¹ Institute of Polymers, Composite and Biomaterials (IPCB), National Research Council of Italy, 80055 Portici, Italy; fabrizia.cilento@ipcb.cnr.it (F.C.); michele.giordano@cnr.it (M.G.)

² CIRA, Italian Aerospace Research Centre, 81043 Capua, Italy; g.giusto@cira.it (G.G.)

³ IMAST S.c.ar.l.—Technological District on Engineering of Polymeric and Composite Materials and Structures, Piazza Bovio 22, 80133 Napoli, Italy

* Correspondence: barbara.palmieri@ipcb.cnr.it (B.P.); alfonso.martone@cnr.it (A.M.)

Featured Application: Multifunctional protective layer for fiber reinforced composites.

Abstract: In the aerospace sector, structural and non-structural composite components are usually subjected to a wide range of environmental conditions. Among all, moisture can seriously damage these materials' performance, reducing their mechanical, thermal, electrical, and physical properties as well as their service time. Lightweight protective barrier coatings capable of reducing the diffusion of gases and/or liquids in a material can improve the material's resistance in humid environments. In this work, nanolamellar nanocomposites characterized by a high in-plane orientation of nanoplatelets have been employed as protective coatings for Kevlar sandwich panels, reproducing the construction of a nacelle engine. The effectiveness of the protection against water uptake of nanocomposites reinforced with graphite nanoplatelets (GNPs) at high filler contents (70, 80 and 90 wt%) has been investigated using moisture uptake and Ground-Air-Ground (GAG) tests in an environmental chamber. GNP coatings effectively work as barrier by generating highly tortuous paths for molecule diffusion. Results showed a dependence of the absorption on the coating composition and inner structure. Films @70 wt% GNPs showed the best protection against moisture uptake by delaying the phenomenon and reducing the absorption by −80% after 3 days and −35% after 41 days.

Keywords: graphite nanoplatelets; moisture uptake; barrier properties



Citation: Cilento, F.; Palmieri, B.; Giusto, G.; Volponi, R.; Bruno, G.; Tartaglia, C.C.; Toscano, C.; Giordano, M.; Martone, A. Graphite

Nanoplatelets Nanostructured Films as Multifunctional Protective Layer in Kevlar/Nomex Sandwich

Composites. *Appl. Sci.* **2023**, *13*, 12812. <https://doi.org/10.3390/app132312812>

Academic Editor: Mark J. Jackson

Received: 29 October 2023

Revised: 24 November 2023

Accepted: 28 November 2023

Published: 29 November 2023



Copyright: © 2023 by the authors. Licensee MDPI, Basel, Switzerland. This article is an open access article distributed under the terms and conditions of the Creative Commons Attribution (CC BY) license (<https://creativecommons.org/licenses/by/4.0/>).

1. Introduction

The use of composite structures in a wide range of fields is still increasing, thanks to their high specific strength and stiffness over metals. The significant weight reduction of these structures translates into a benefit for the industry in terms of cost savings and environmental benefits, especially in terms of fuel savings [1], with the recycling phase of the composites remaining the key environmental issue. However, it is well known that the mechanical properties of fibre-reinforced composites can be very sensitive to environmental parameters. Temperature, humidity, light, or environmental impact phenomena such as rain, lightning, or hail affect the durability of composite materials, becoming a crucial issue when they are used as structural materials [2]. These severe environmental conditions can limit the use of polymeric composites, especially for applications in which high performances are required. In an aircraft, some primary structures are always subjected to varying temperature and moisture exposures throughout their entire service life. Continuous exposure to high temperature and moisture levels may lead to a change in the mechanical behaviour of the aircraft's structural components [3,4]. Furthermore, cyclic thermal, moisture and mechanical loadings could even further deteriorate the performance of the structures leading to premature failure. These environmental conditions,

especially temperature and moisture exposure, vary widely during a flight from the take-off to the landing.

Specifically, Kevlar-reinforced composites are prone to moisture uptake, due to the strong hygroscopic nature of both the resin and the fibre. Epoxy resins are strongly sensitive to water absorption because of large amounts of polar OH groups in the networks which facilitate attractive interactions with polar molecules of water [5–7]. It was found that the maximum moisture absorption for epoxy is 2 wt% at 70 °C and 100% RH [8] and 6 wt% for Kevlar 49 aramid fibres when they are exposed to a high-humidity environment (96% RH) [9]. The absorbed moisture leads to the plasticization phenomenon in the matrix resin, decreasing the glass transition temperature and also generating changes in the state of stress in favour of cracking through swelling [10–12], degrading the mechanical properties of the material [2–4]. As a consequence, the stress transfer at the fibre-matrix interphase is compromised and the overall behaviour of the composite becomes more brittle: the impact strength and fracture toughness can even drop by 50% [13].

In aerospace applications, the use of Kevlar honeycomb sandwiches is widespread, thanks to their excellent mechanical performances, i.e., their high bending-stiffness-to-weight ratio [14]. Nevertheless, the honeycomb core absorbs water via the capillary phenomenon [15,16]. The moisture locally accumulates inside the honeycomb cells, thereby jeopardising the original purpose of adopting sandwich structures for weight reduction and seriously affecting the integrity of composite structures and aircraft safety [17,18]. The industrial solution currently used is based on aluminium paints applied through a flame-spray technique, thanks to the combined barrier effect against water adsorption and antistatic properties [19–21]. Although these barrier films have a water vapor transmission rate (WVTR) equal to $\sim 10^{-1}$ g/m²h [22–24], they also have some drawbacks, i.e., their high weight and fragility [25]. Alternatively, polymer-based films, such as polyvinyl fluoride (PVF) films, are extensively used in aerospace applications thanks to their low permeability of 24.5 g/m²day for vapours and low ignition time [26,27]. These hydrophobic films are usually co-bonded to surfaces of the glass, carbon, and Kevlar composite structures, providing a moisture absorption <0.5% [28].

In the last decade, the possibility of using graphite nanoplatelets (GNPs) to improve the barrier properties of polymers has been investigated [29]. These nanoparticles are promising nanomaterials in gas- or liquid-barrier applications because graphene sheets do not allow the diffusion of small gases or liquids through their plane. To fulfil this function, films with special architecture can be employed as lightweight protective coatings for composites [30]. Nanoarchitectures with a high level of nanoplatelet orientation and high nanofiller content (>50 vol%) ensure a high tortuosity factor, resulting in high barrier and low permeability properties [31,32]. Recent studies showed that highly aligned graphene fillers in polymeric coatings can reduce transmission rates by nearly 400 times compared to neat polymer [33]. Further, films at 80 wt% nanofiller content showed a reduction of the WVTR of nearly 90% [34].

Moreover, GNP films with this architecture are also employed for other applications. Indeed, the intrinsic properties of the nanoplatelet (i.e., good thermal and electrical conductivities) are scaled on the macroscale when assembled in a well oriented nanostructure. GNP films have been widely used in thermal management applications [35,36], such as heating elements in innovative de-icing systems [37,38], thermal barrier coatings of carbon fibre composites and heat spreaders in battery packs [39], thanks to the high thermal conductivity, which can vary between 600 to 3200 W/mK according to the production process [40]. Additionally, films with a good orientation and superposition of GNPs ensure high electrical conductivity (in the order of 10^3 – 10^5 S/m) and can be used as electromagnetic shielding materials [41]. Indeed, Wei et al. reported that the well-aligned structure of GNP films is not only beneficial for high electrical conductivity but also favourable for multiple internal reflections of electromagnetic waves, resulting in a shielding effectiveness of about 90 dB [42]. Thin and highly conductive GNP films are also employed to reduce the effects of lightning on composite aircraft, reducing delamination [43,44]. Wang

et al. demonstrated that a highly electrically conductive graphene coating on the surface of carbon fibre composites facilitates lightning's electrical current to spread out without significant damage [45].

In this work, the authors investigated the possibility of employing high-content nanocomposites made with GNPs as a protective layer for reducing moisture absorption. GNP films with high filler content have been integrated into Kevlar/epoxy panels in a one-step manufacturing process. Panels have been fabricated with protective layers at different filler contents (70, 80, 90 wt%). The effectiveness of protection against water uptake has been investigated through moisture uptake and GAG tests in an environmental chamber and the level of damage in the panels has been investigated with non-destructive inspection (NDI). Results indicate that GNP films are effective in protecting the panel from moisture, with a reduction of the maximum absorption after 40 days of 30%. The easy integration of these films in the manufacturing process of composites in a co-curing process ensures a reduction in the processing time and improves energy savings.

2. Materials and Methods

2.1. Materials and Manufacturing Procedure

Kevlar/Nomex sandwich panels were selected, since they are commonly employed in the construction of engine nacelles. Square samples of 180 mm side were fabricated, with a tapered core with an angle of $18^\circ \pm 3^\circ$, such that the footprint varied from $140 \times 140 \text{ mm}^2$ to $50 \times 50 \text{ mm}^2$ on the lower and upper surfaces, respectively (Figure 1).

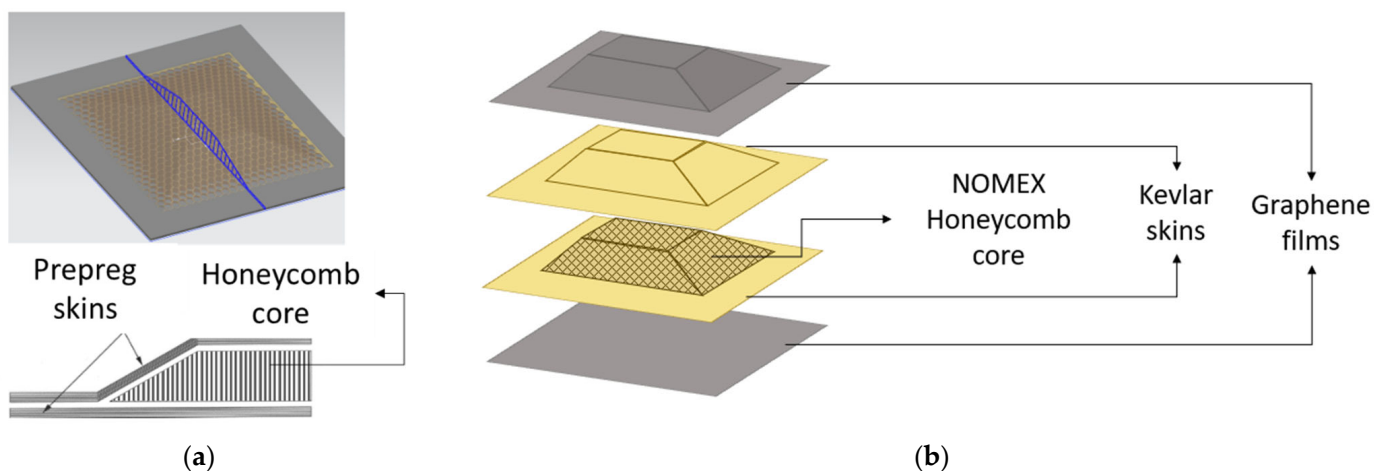


Figure 1. Geometry of the Kevlar sandwich panel (a) and stratification (b).

The GNPs considered in this study were kindly supplied by NANESA S.r.l. A single platelet has a lateral size of $30 \mu\text{m}$ and thickness of 14 nm , and an aspect ratio of 2143. The GNP-rich films were fabricated following a top-down approach, based on a spray deposition process. These self-standing films were pre-impregnated with a monocomponent epoxy resin (Hexcel RTM6) at different contents (10, 20, 30 wt%). Details of the fabrication process are reported in previous work [46]. Films had a thickness of $70 \pm 6 \mu\text{m}$ and a weight of $80\text{--}90 \text{ g/m}^2$.

To evaluate the effectiveness of the GNP layer in reducing water uptake, uncoated and coated Kevlar sandwich panel samples were fabricated. Seven panels were manufactured, including three pairs of panels coated with films with different GNP contents (70%, 80%, 90%) and one reference sample without protection, and are listed in Table 1.

Table 1. List of fabricated panels.

Panel ID	Description
P-REF	No coating
P70-A; P70-B	70 wt% GNP coating
P80-A; P80-B	80 wt% GNP coating
P90-A; P90-B	90 wt% GNP coating

The manufacturing process of the panels was carried out in the following steps, and described in Figure 2a:

- (i) Stacking of the lower skin according to the layout sequence (0/90)₄.
- (ii) Core positioning, where the core was prepared according to the final geometry before lamination.
- (iii) Stacking by prepregs the core contour (0/90)₆ and the upper skin (0/90)₄.
- (iv) Curing in an oven for 2 h at 120 °C in a vacuum bag.

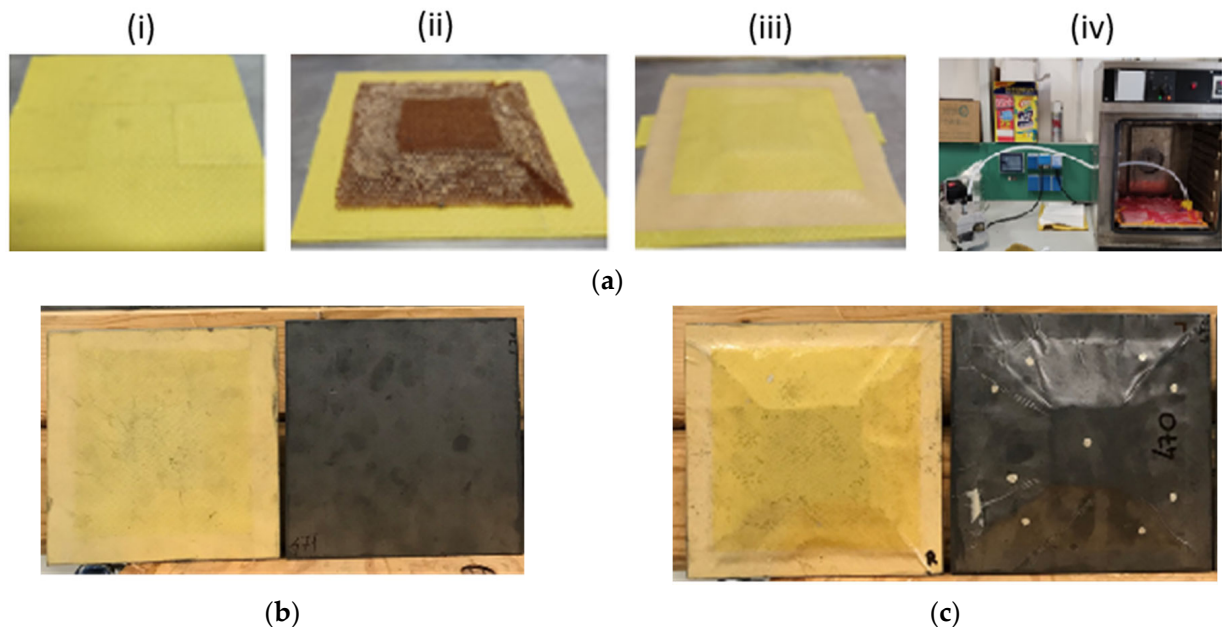


Figure 2. Panel manufacturing phases stacking, and vacuum bagging cure (a); External surfaces of both uncoated and coated samples (b,c).

Finally, panels were trimmed and sealed on the edges. The GNP films on both the lower and upper surfaces were considered as additional layers in the stacking (i.e., tool side layer in the lower skin, and last layer in the upper skin).

2.2. Experimental Characterization

Thermogravimetric analysis (TGA) (TA Instruments Q500) was conducted to evaluate the real filler/matrix composition of the GNP-rich films. Measurements were performed in an inert atmosphere, using nitrogen gas, with a temperature ramp of 10 °C/min from room temperature to 800 °C. The weight loss was evaluated at 600 °C, the temperature at which the resin residue was 10.3%.

The electrical resistivity of the GNP films was assessed using the Keithley 6221 picoammeter and the Metex M3850D digital multimeter. The picoammeter was used to generate currents with different densities in the 1–100 mA range, while the multimeter was used to monitor the voltage. The measurement was conducted on rectangular samples of 5 cm × 1 cm size and a silver conductive paste was used to facilitate the measurement. To

prevent the samples from breaking during the measurements, they were reinforced with transparent adhesive tape.

To assess the effect of protection of the GNP films, a moisture uptake test was performed according to ASTM D5229 [47]. All samples listed in Table 1 were placed in a climatic chamber (Angelantoni CH 2000) at a controlled temperature of 70 °C with a relative humidity of 85% for 40 days, as shown in Figure 3a. The increase of weight with time was measured by weighing the panels at different time steps. To avoid undesired movements of the specimens during the test, the panels were fixed on a metallic grid using four bolts accurately covered with tape (Figure 3b,c). Before starting the test, the panels were conditioned in a vacuum oven at 80 °C for 3 weeks in order to remove any traces of moisture and fix the same starting point. The samples were weighed every 3 days in the first week and then every week, as indicated in Table 2. Before each weighing, samples were dried with a paper towel to eliminate the excess water. The measurements were repeated three times, and the average value was computed and registered.

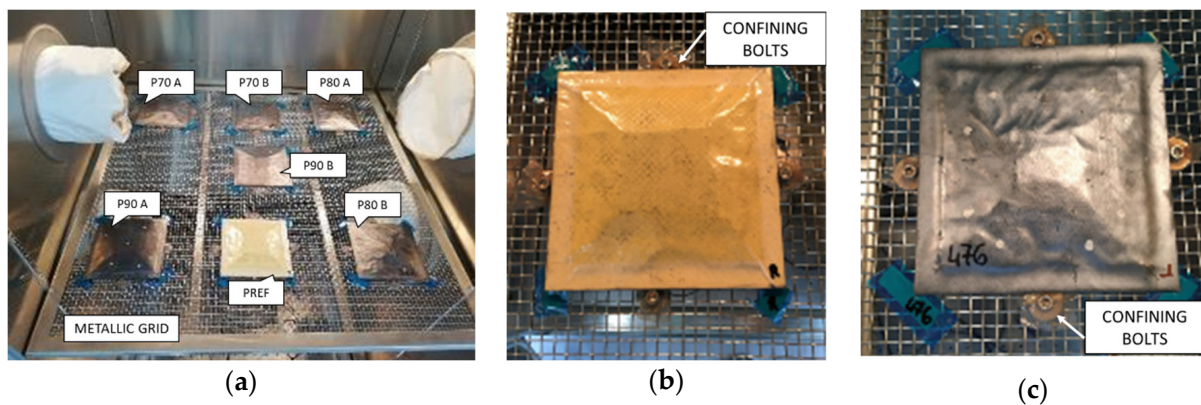


Figure 3. (a) Panels positioning on the metallic grid; (b) Uncoated panel; (c) GNP coated panel.

Table 2. Weighing schedule for moisture uptake test.

Weight	Time (Days)	Time (Hours)
W_0	0	0
W_1	3	72
W_2	6	144
W_3	13	312
W_4	20	480
W_5	27	648
W_6	34	816
W_7	41	984

Finally, non-destructive inspections (NDI) were conducted to investigate the internal structure of the panels using lock-in thermography [48]. This technique exploits the thermal response of the material when subjected to specific thermal waves: if the waves encounter an obstacle (defect), their normal diffusion is prevented. The investigation depth is strictly related to the thermal wave frequency: high frequencies limit the analysis to regions close to the surface, while low frequencies propagate to greater depths. Analyses were conducted before and after the test to assess the potential damage of the samples when placed in a moist environment at 0.1 Hz and 0.04 Hz.

3. Results

3.1. GNPs-Protective Coating Functional Properties

The real GNP contents have been assessed using TGA analysis and the thermograms are reported in Figure 4. The major weight loss occurs between 350 °C and 500 °C and

it is associated with the epoxy resin degradation. The residual reached its plateau at about 600 °C. The obtained results confirmed the correspondence between nominal and actual GNP content in the films. The real filler content, $w_{f,real}$, is computed according to Equation (1) and the results are reported in Table 3.

$$w_{f,real} = \frac{R_i - R_m}{100 - R_m} \% \quad (1)$$

where R_i is the residue from TGA at 600 °C of the sample and R_m is the residue of the pure epoxy resin equal to 10%.

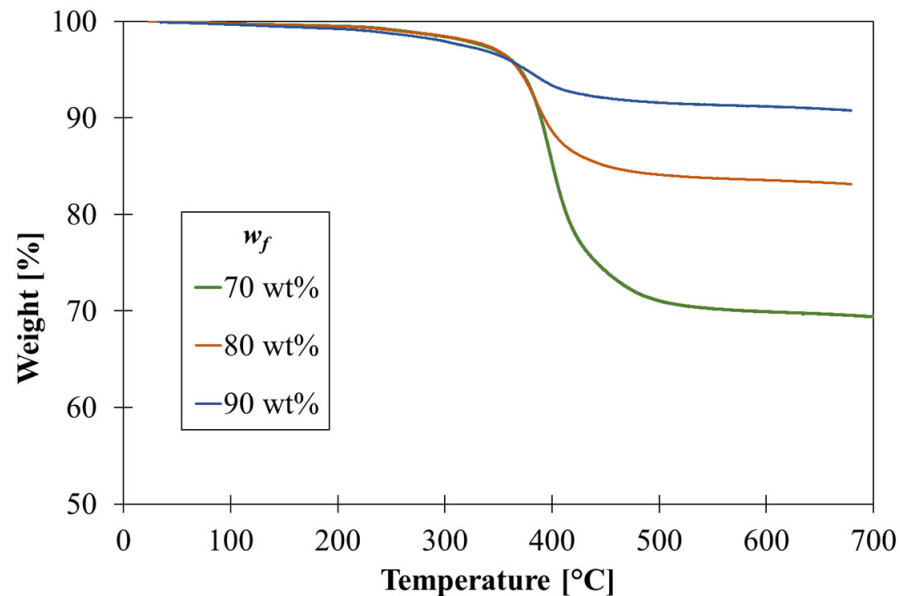


Figure 4. TGA curves of films at different GNP content.

Table 3. Results of TGA and values of filler contents.

$w_{f,nominal}$ [wt%]	R_i [wt%]	$w_{f,real}$ [wt%]
70	72	69
80	86	84
90	91	90

The electrical resistance (R) of the GNP-rich films with different filler contents was measured with a voltage amperometric test. The resistivity ρ [Ωm] was computed according to Equation (2), where R is the measured resistance and w and L are the width and length of the sample.

$$\rho = R \cdot \frac{w \cdot t}{L} \quad (2)$$

The films exhibit low electrical resistivity, which slightly decreases with increasing filler content as reported in Table 4. In addition, these values are compatible with the electrical resistivity of graphite (1.3×10^{-5}), which represents the theoretical natural limit [49]. The GNP coating also improves the panels' electrical conductivity, providing, as an additional feature, the dissipation of the electrostatic discharge (ESD) that can accumulate on the surface [50,51].

Table 4. Values of electrical resistivity of GNP films.

Filler Content [wt%]	Resistance, R [Ω]	Width, w [mm]	Length, L [mm]	Thickness, t [μm]	Resistivity, ρ [Ωm]
80	4.70	10	55	72	8.54×10^{-5}
85	3.49	11	57	71	6.75×10^{-5}
90	1.82	16	40	73	4.96×10^{-5}

3.2. Moisture Diffusion in Sandwich Plates

The sorption curves of the Kevlar/epoxy sandwich with and without the protection are shown in Figure 5, where moisture uptake is plotted against the square root of time. The moisture uptake, M , is evaluated according to Equation (3) [47]:

$$M(t) = \frac{W(t) - W_0}{W_0} \times 100\% \tag{3}$$

where W_0 is the panel weight at time $t = 0$, before starting the test, and $W(t)$ is the weight of the panel at each weighing step of Table 2.

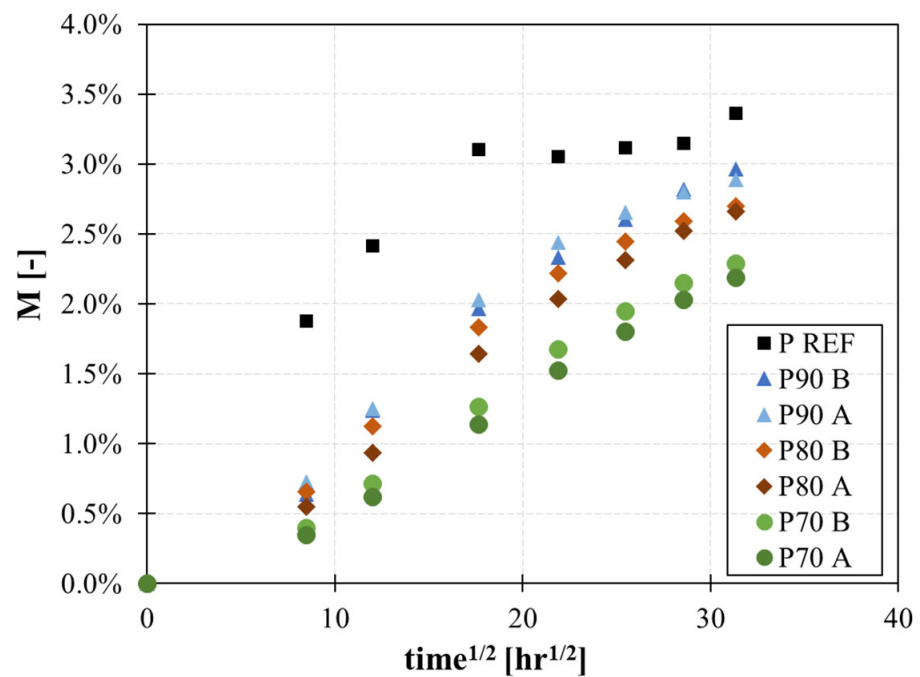


Figure 5. Moisture uptake with time of uncoated and coated panels.

Results show that the GNP layer improves the resistance to moisture uptake, both in terms of maximum absorbance and diffusion rate. A reduction of 30% of the maximum moisture absorption has been observed in protected samples with respect to the reference Kevlar/epoxy sandwich (Table 5). The GNP layer also modifies the absorption curve. In the uncoated panel, the absorption rate is higher and the saturation is reached earlier compared to coated panels. The presence of the GNP films lowers the absorption rate, thanks to the tortuous path created by the well-oriented nanoparticles.

Table 5. Maximum moisture uptake after 41 days and water diffusivity at 3 days ($t = 259,200$ s) for tested panels.

Panel ID	$w_{f,real}$ [%]	M @ 41 Days [%]	$\Delta M/\Delta M_{max}$ @ 3 Days [-]	D [m^2/s]
P REF	-	3.4 ± 0.11	0.55	3.8×10^{-12}
P70 A	70	2.2 ± 0.07	0.16	3.0×10^{-13}
P70 B	70	2.3 ± 0.05	0.17	3.7×10^{-13}
P80 A	77	2.7 ± 0.13	0.21	5.2×10^{-13}
P80 B	86	2.7 ± 0.09	0.24	7.2×10^{-13}
P90 A	91	2.9 ± 0.06	0.25	7.7×10^{-13}
P90 B	91	3.0 ± 0.08	0.26	8.0×10^{-13}

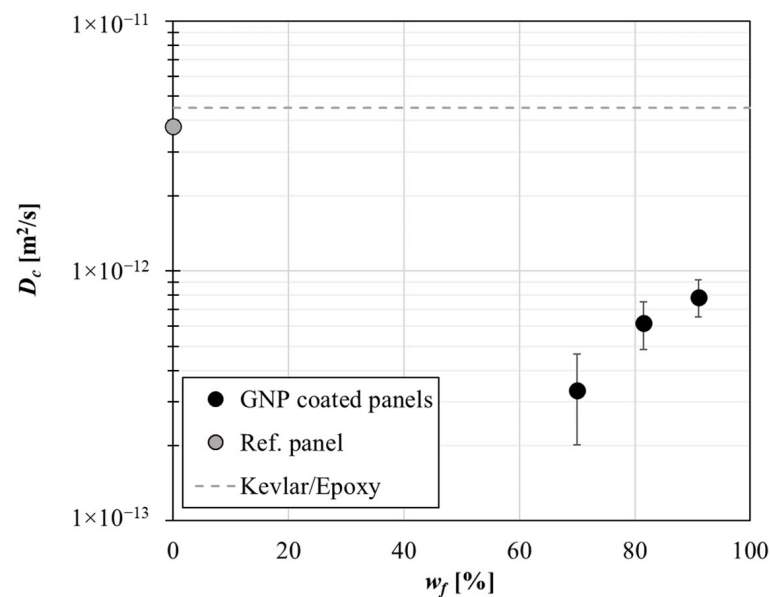
Furthermore, the material's diffusivity (D) has been calculated from the results of the moisture uptake test as a function of time, according to Fick's second law. It describes the time-dependent absorption of a gas or liquid into a sheet by accounting for accumulation into the material. If a gas or liquid is absorbed in a homogeneous and infinitely long sheet, an increase in mass (ΔM) occurs as a function of time (t) until saturation (ΔM_{max}). At short times ($Dt/h^2 < 0.06$, or equivalently $\Delta M/\Delta M_{max} < 0.55$), Fick's second law can be approximated to a linear relationship between the relative mass gain and the square root of time (Equation (4)) [52].

$$\frac{\Delta M}{\Delta M_{max}} = \frac{4}{\sqrt{\pi}} \cdot \sqrt{\frac{D \cdot t}{h^2}} \quad (4)$$

$$D = \frac{\pi}{16} \cdot \frac{h^2}{t} \cdot \left(\frac{\Delta M}{\Delta M_{max}} \right)^2$$

where $\Delta M/\Delta M_{max}$ is the relative change in mass, and t and h are the time and the thickness of the sample, respectively.

A sensible reduction of the water diffusivity is found for protected panels, as shown in Figure 6. In the case of the unprotected panel, the diffusivity is $3.8 \times 10^{-12} m^2/s$, consistent with data reported in the literature [53]. When a GNP coating is applied, the diffusivity reduces by an order of magnitude, as shown in Figure 6. This reduction depends on the GNP content: a minimum value is observed in the case of P70 with a -90% reduction compared to P REF. By increasing the GNP content, the efficiency of protection of the coating reduces; the diffusivity in P90 reduces by -80% compared to the reference.

**Figure 6.** Water diffusivity vs. filler content in the panels at 3 days.

4. Discussion

4.1. Influence of Filler Content on Water Uptake

Once the moisture is absorbed on the upstream surface of the material, it diffuses across the thickness of the protective films and penetrates the panel, accumulating in it. The use of a protective coating with nanolamellar architecture showed a significant reduction of the moisture uptake and the absorption rate.

The efficacy of protection against water uptake (η) has been estimated according to Equation (5).

$$\eta = \frac{M_P - M_{Ref}}{M_{Ref}} \quad (5)$$

where M_P and M_{Ref} are the values of the moisture uptake in the coated panel and in the reference panel after 3 days and 41 days, respectively. The parameter η represents the mass uptake saved with respect to the unprotected system.

The data of efficiency are reported in Table 6 for all the analysed panels. It is at maximum for panels protected with 70 wt% of GNPs and then decreases with filler content, both at 3 days and 41 days. Further, the efficacy is higher at shorter periods of time, highlighting that the protective coating not only reduces the maximum moisture uptake at saturation but slows the absorption phenomenon over time.

Table 6. Effective protection against moisture uptake at 3 days and 41 days.

ID	η (t = 3 Days)	η (t = 41 Days)
P70 A	$-82 \pm 3\%$	$-35\% \pm 4\%$
P70 B	$-79\% \pm 2\%$	$-32\% \pm 6\%$
P80 A	$-71\% \pm 4\%$	$-21\% \pm 2\%$
P80 B	$-65\% \pm 3\%$	$-20\% \pm 2\%$
P90 A	$-61\% \pm 4\%$	$-14\% \pm 5\%$
P90 B	$-61\% \pm 5\%$	$-14\% \pm 3\%$

The hydrophobic nature of GNPs, combined with the very high in-plane orientation of nanoplatelets and the low matrix content, creates an impervious path for vapour and gases [54]. For a material filled with nanoplatelets, oriented perpendicular to the diffusion direction, the diffusivity depends on the matrix diffusivity and on the path that the molecules follow when they cross the two phases [55]. The longer the distance travelled by the diffusing molecule across the film's thickness, the more tortuous the pathway. Zeng et al. found that the lateral size of the nanoplatelet influences the permeability of the film, and a high lateral size of nanofiller results in a low transmission rate [56].

A tortuosity factor (τ) is defined in Equation (6) for nanocomposites reinforced with lamellar-oriented nanoplatelets, which depends on the filler aspect ratio (AR) and volume fraction (v_f) [55]. It increases with the volumetric filler fraction, reducing asymptotically to zero.

$$\tau = 1 + \frac{AR}{2} \cdot v_f \quad (6)$$

According to Equation (6), the tortuosity factor in the case of GNP films loaded with 70, 80, and 90 wt% of GNPs are computed and listed in Table 7. By increasing the nanofiller content, the nanoarchitecture of the films, composed of highly oriented nanoplatelets, should force the water molecules to move in an increasingly tortuous path, resulting in a reduction of diffusion through the protective film.

Table 7. Tortuosity factor in GNPs/epoxy nanocomposites (with $AR = 2143$).

$w_{f,real}$ [wt%]	v_f [vol%]	τ [-]
68.8	52.2	560.3
84.4	72.8	781.3
90.0	81.6	875.6

On the contrary, experimental data showed that in panels coated with GNP films, the absorption depends on the coating composition and increases with an increasing nanofiller content. The lowest absorption is found in the panel protected with film @70 wt% of GNP.

A rationale for this behaviour is found in the material's inner architecture. Morphological observations of previous works have revealed a maximum level of compaction in nanocomposites with 70 wt% of GNPs [57]. By increasing the filler content up to 90 wt%, the nanostructure is modified by the presence of dry spots and voids, as shown in the SEM images in Figure 7. The matrix phase at high filler contents appears to be discontinuous, partially covering the nanoplatelets' surface [46,58]. These uncovered areas may be detrimental to the barrier effect. Although the water molecules travel a more impervious path, they cross areas with different diffusivities (air and matrix), resulting in a higher absorption (Figure 7).

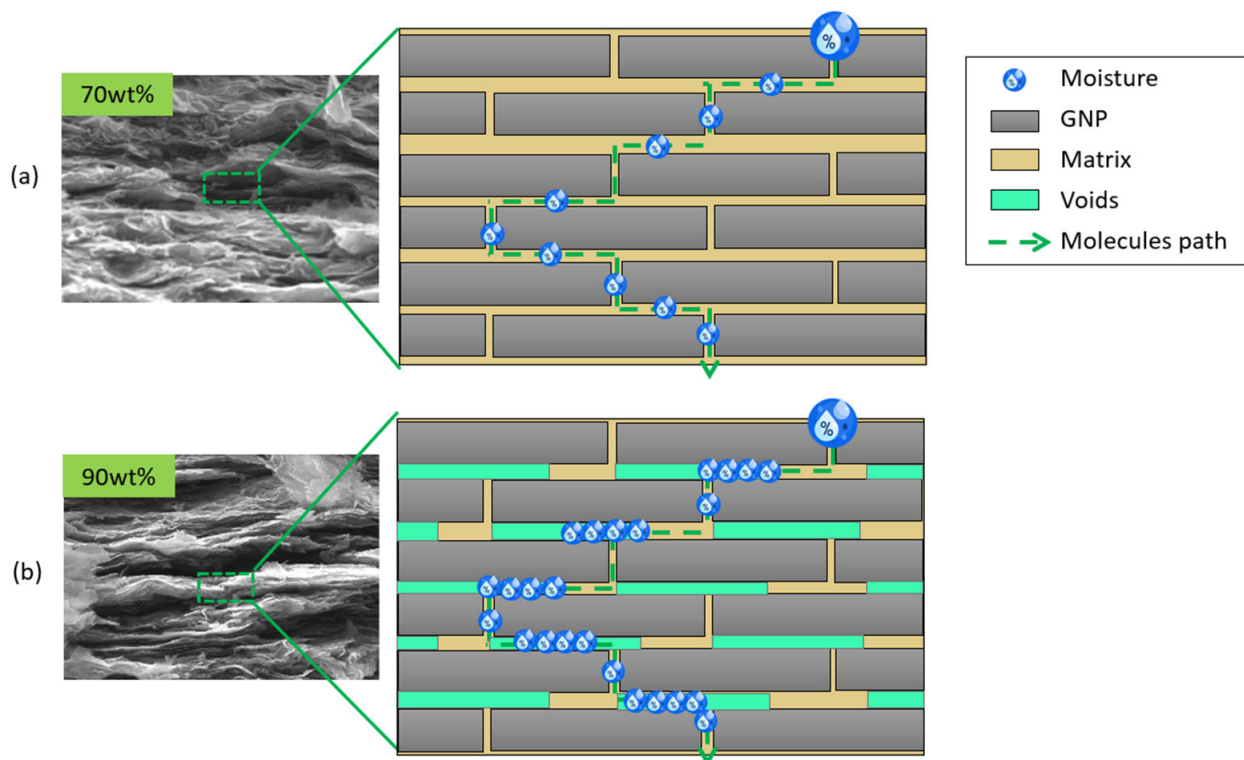


Figure 7. SEM images of GNP films and sketches of their architecture at various filler contents: (a) 70 wt% and (b) 90 wt%.

Therefore, the moisture uptake in panels protected with GNP films with 90 wt% filler content is higher than that of panels coated with GNP films with 70 wt% filler content. However, this value is significantly lower than that of the uncoated panel (3.4%).

Further investigations based on contact angle measurements demonstrated that films @90wt% of GNPs have more hydrophilic behaviour compared to films @70 wt% of GNPs, as shown in Figure 8. Analyses are conducted using optical contact angle measuring (OCA 20 DataPhysics) and contour analysis systems, using distilled water drops of 1 mL. Figure 8

reports the contact angle (θ), geometrically defined as the angle formed between the liquid and the solid surface.

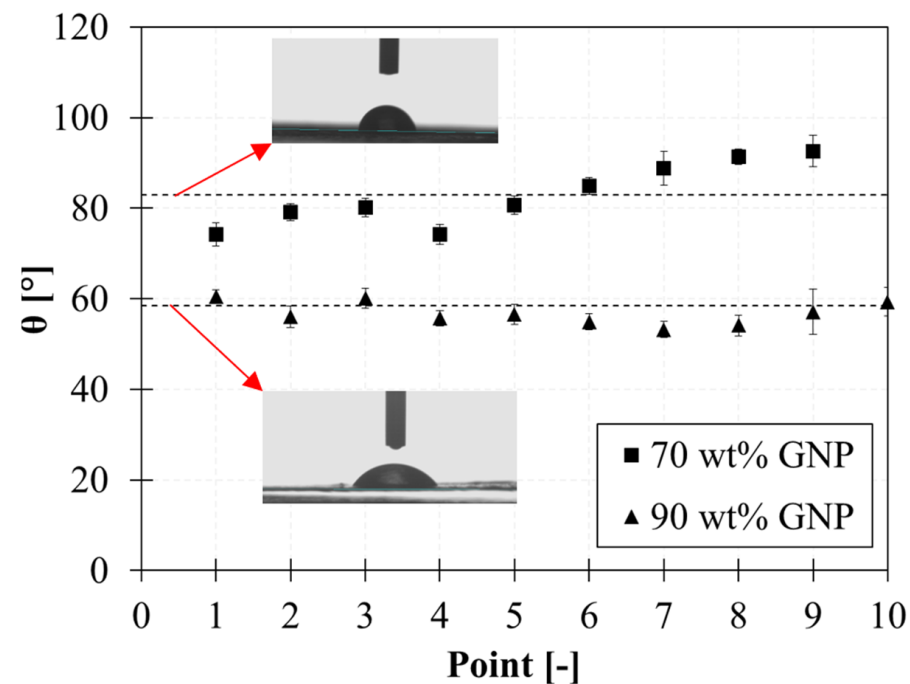


Figure 8. Contact angle measurements on films @70 wt% and 90 wt% f GNPs.

An average contact angle of 83° and 59° is found for films with 70 wt% and 90 wt% of GNPs, respectively, confirming that, by changing the GNP content, the surface properties have been modified. Since the GNP content also affects the inner architecture (tortuosity) of the protective layer, even the cross-permeability has been modified [59,60]. These results indicate that the wetting states of membranes influence their permeability and corroborates the hypothesis that nanocomposites become more inclined to water absorption with increasing GNP content.

4.2. Ground-Air-Ground (GAG)

The Ground-Air-Ground (GAG) test was performed to assess the performance of the material during flight. The test consists of subjecting the specimens to the combined effects of temperature, pressure, and relative humidity, thus reproducing flight conditions. The GAG test was conducted using the same combined environmental chamber used for the moisture uptake test, and the samples were tested for 10 repeated cycles. The test procedure is shown in Figure 9. In accordance with ASTM D5229 [47], samples were subjected to a rapid temperature drop to -54°C , followed by a rapid temperature rise to 70°C , under conditions of maximum moisture saturation (95% RH). Specifically, each cycle has a duration of 240 min and follows the following steps:

1. Parking the aircraft on the ground in a cool environment: lower the chamber temperature to -54°C at a rate of $5^\circ\text{C}/\text{min}$ and keep these conditions for 45 min.
2. Lowering the chamber pressure to 120 mbar with a minimum temperature of -54°C . This condition represents the take-off up to 15,000 m with a maximum ascent rate. Keep these conditions for 40 min.
3. Increase the pressure to 1013 mbar and raise the temperature to 70°C simulating landing in a warm environment and parking on the ground at 70°C for 25 min.
4. Increase relative humidity to 95% and remain in this condition (70°C and RH 95%) for 60 min (park on the ground in a hot, humid environment).
5. Return chamber conditions to 20°C and 50% and remain for 10 min.

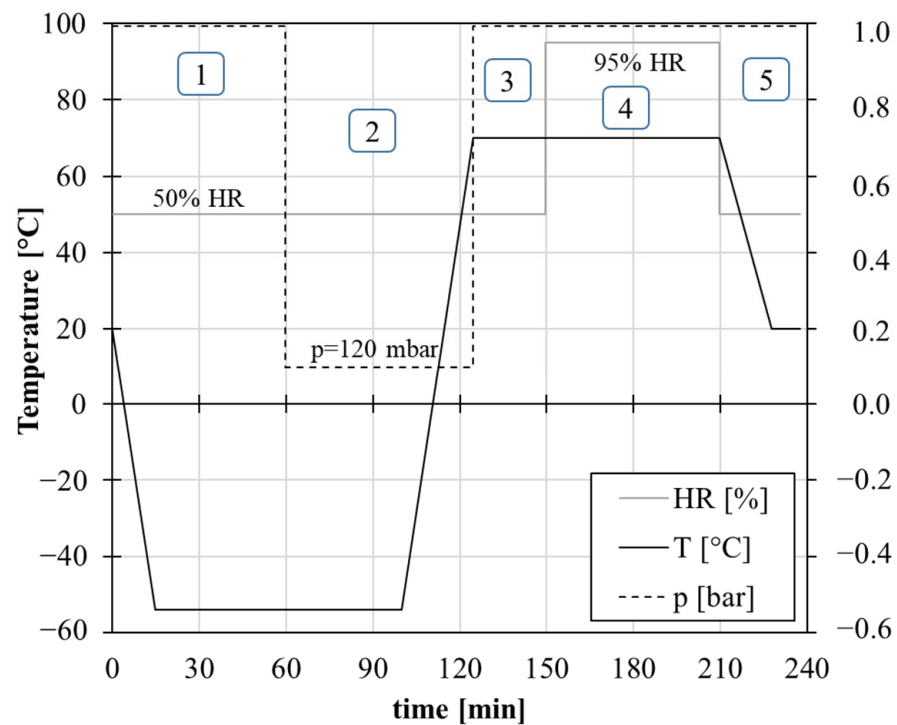


Figure 9. GAG test: temperature, humidity, and pressure profiles.

All panels were subjected to the GAG test. Before starting the test, all samples were dried in a vacuum oven at 80 °C for 3 weeks and weighed. Further weighing was done after the first and tenth cycles.

After ten cycles, the maximum absorption in panels coated with the GNP layer was sensibly reduced, as well as their absorption rate. The barrier effect decreases with increasing GNP content: sample P70 showed the lowest value of absorption. Results of the GAG test conducted on panels are reported in Table 8 in terms of moisture uptake.

Table 8. Moisture uptake during the GAG test for each panel.

Panel ID	M @ Cycle 1 [%]	M @ Cycle 10 [%]
P REF	0.59 ± 0.05	1.81 ± 0.08
P70	0.07 ± 0.01	0.28 ± 0.08
P80	0.18 ± 0.03	0.64 ± 0.04
P90	0.17 ± 0.06	0.68 ± 0.09

During the GAG test, the integrity of the GNP layer on the surface was monitored by measuring the electrical conductivity of the layer. Two electric wires were fastened with a conductive paste on the diagonal of each specimen and the different specimens were connected in series, as shown in Figure 10. The samples were fed with a 100 mA current, and voltage was recorded across each sample.

The results of the surface resistance measurements of specimens during the GAG test, until the 10th cycle, are reported in Figure 11. The resistance slightly increased during the test for all samples due to water absorption, as reported in Figure 12.

By comparing the results of the moisture uptake and GAG tests, similar behaviours between GNP coating compositions are found, as shown in Figure 13. In the case of the moisture uptake test, after 72 h the absorption sensibly reduces in the panels coated with GNP layers compared to the uncoated panel by −71% for P70, −61% for P80, and −41% @90 wt% for P90. Likewise, in the case of the GAG test after 40 h the panel absorption reduces by −85% for P70, −65% for P80, and −63% for P90 compared to P REF.

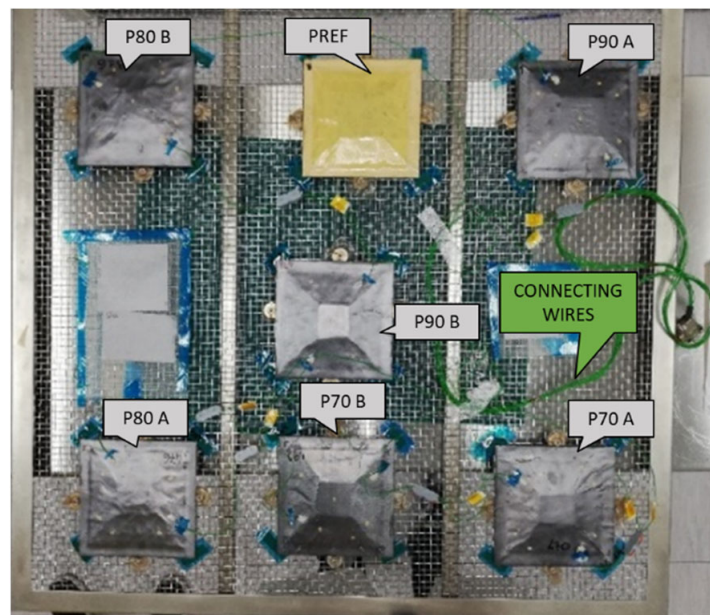


Figure 10. Kevlar sandwich panel samples: positioning in the chamber and set-up for electrical conductivity measurements.

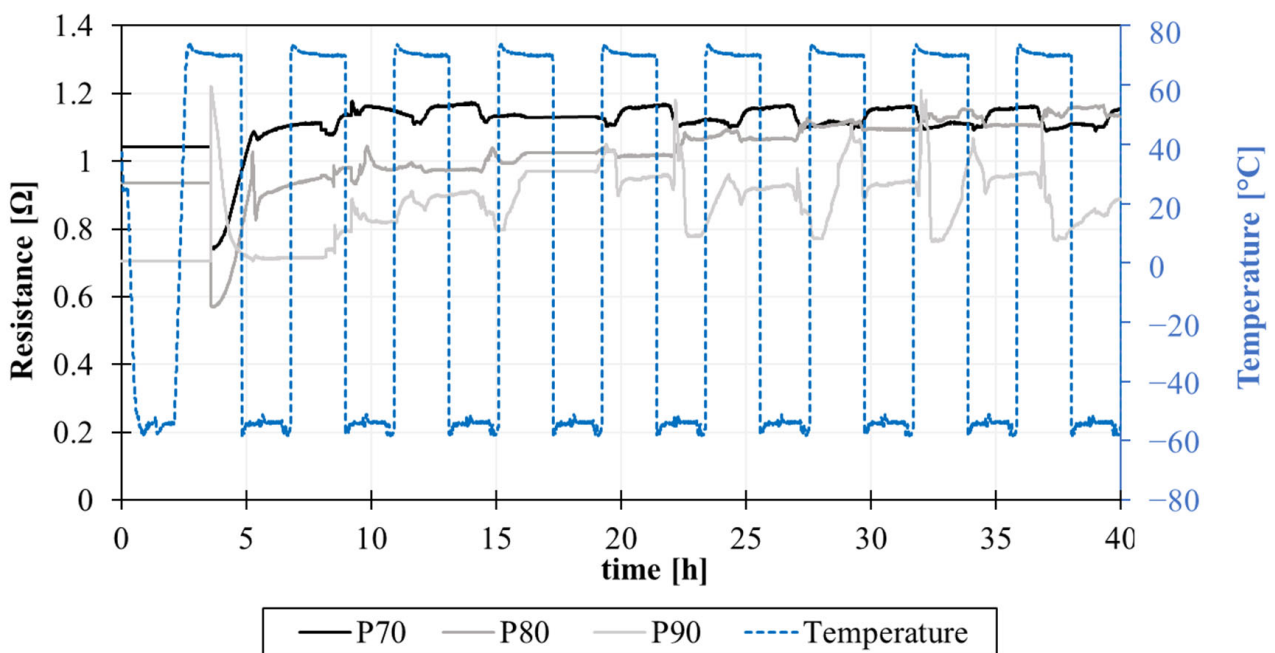


Figure 11. Electrical resistance vs. time for each panel during the 10 cycles (40 h) of the GAG test.

4.3. Non-Destructive Inspection of Sandwich Plates

Non-destructive inspections on specimens before and after the moisture uptake test revealed that the panels did not experience damage. Figures 14 and 15 show the results of the NDI analysis conducted on the lower surface of the samples at different frequencies of 0.1 Hz and 0.04 Hz. By decreasing the frequency, different depths of the samples are investigated, and at 0.04 Hz it is even possible to observe the taper of the inner core. By comparing the images of samples before and after the test, for both sampling frequencies, it appears that the induced stress of the moisture uptake test did not produce any damage. Analogous results are obtained from the NDI after the GAG test. The induced stress of flight cycle simulations did not cause internal damage.

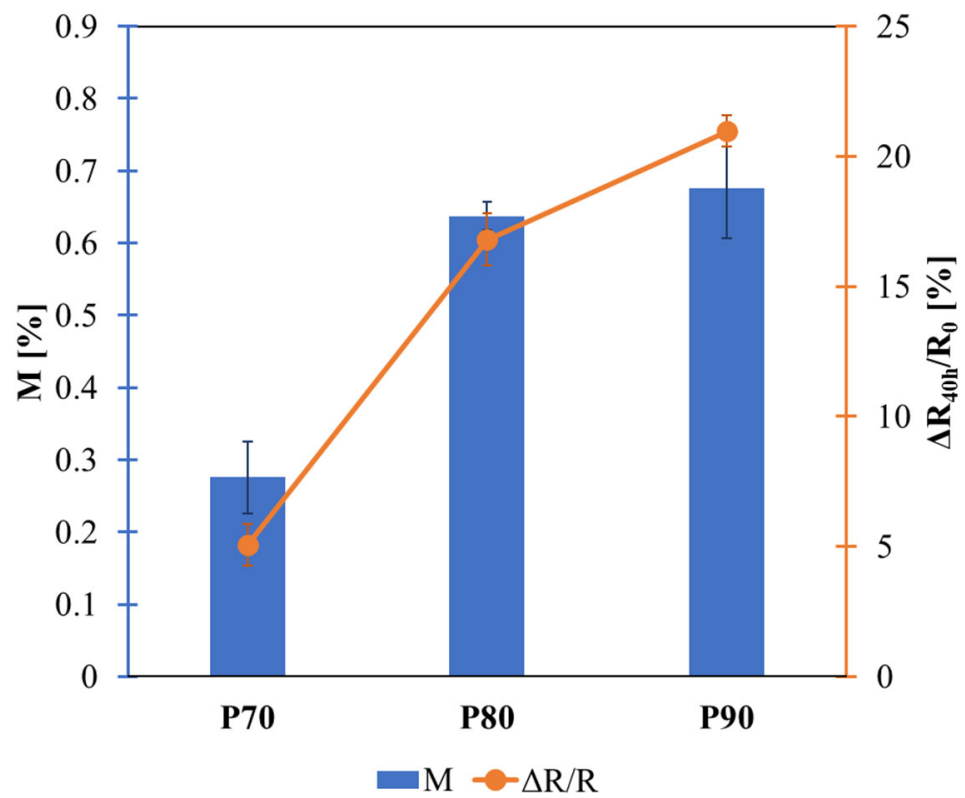


Figure 12. Trend of moisture uptake and variation of resistance at the end of the GAG test.

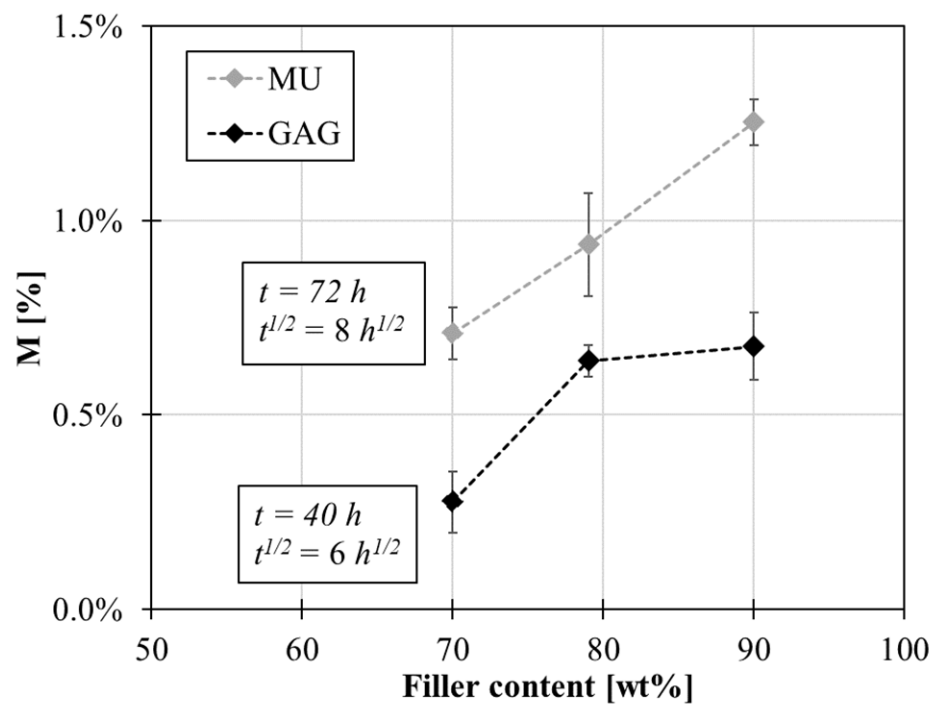


Figure 13. Comparison between moisture uptake (MU) and GAG tests.

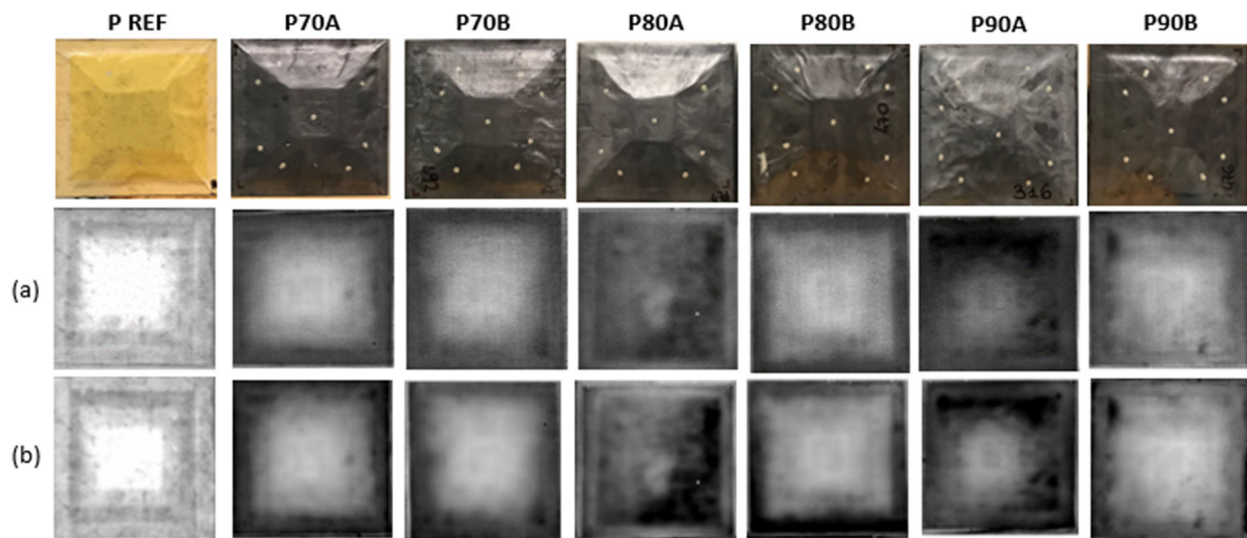


Figure 14. Thermal images: (a) before performing the test; (b) after the moisture uptake test at 0.1 Hz.

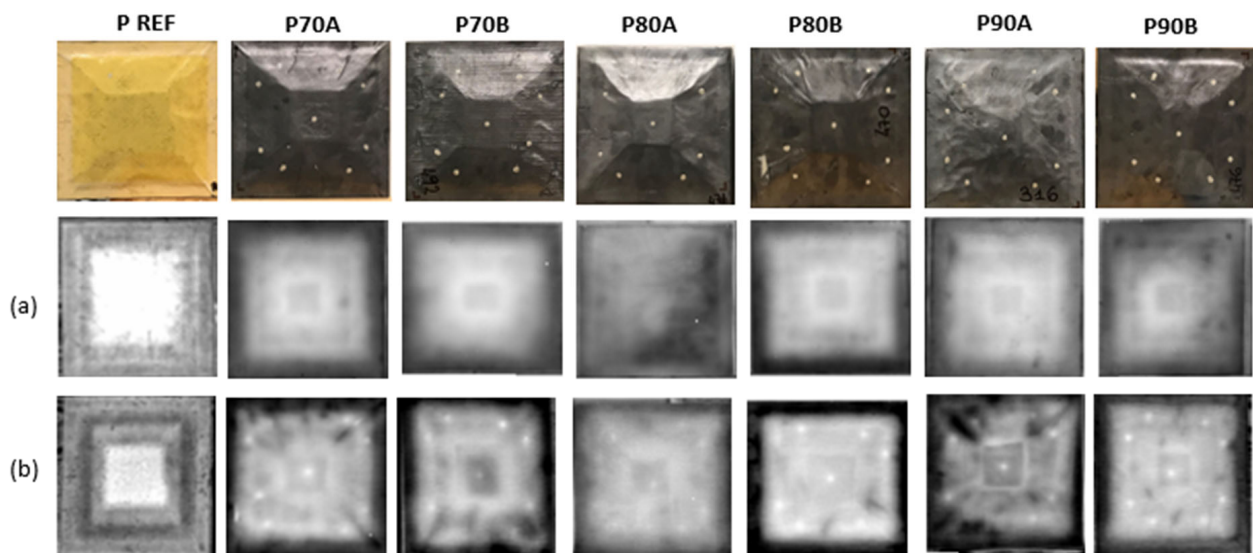


Figure 15. Thermal images: (a) before performing the test; (b) after the moisture uptake test at 0.04 Hz.

5. Conclusions

The effectiveness of the protection against moisture uptake of GNP-rich films has been investigated through a moisture uptake test in an environmental chamber. The behaviour of Kevlar sandwich panels, representative of a regional aircraft composite part, in a humid environment, has been investigated, and the ability of GNP films to protect Kevlar/epoxy panels from water absorption has been demonstrated.

After 41 days in a humid environment, the maximum sorption is reduced by -35% in samples protected with films @70 wt% of GNPs, compared to the unprotected system. Moreover, an evident delay in the absorption rate into the composite panels due to the presence of the protective layer has been observed, with a reduction of -80% after 3 days. A Ground-Air-Ground (GAG) test has been carried out to reproduce the actual flight envelope. The GAG test showed that after 10 cycles, the maximum sorption of the panel coated with a film @70 wt% of GNPs is about 70% lower than that of the uncoated one. NDI analysis with lock-in thermography revealed the absence of damage in all panels after the test.

The nanocomposite nanostructure plays an important role in the barrier's properties, reducing the absorption rate and the maximum moisture uptake. The GNP protective films reported an efficiency against moisture absorption between 80% and 62% at short times

(3 days) and between 35% and 14% at saturation, based on the filler/matrix composition. Thanks to the nanoplatelet alignment and the intrinsic hydrophobicity of GNPs, the film acts as barrier to moisture regardless the nanofiller content, with a diffusivity coefficient of the same magnitude of aluminium ($\sim 10^{-12} \text{ m}^2/\text{s}$) [61].

However, the overall behaviour is affected by the filler content. Although the theoretical model indicates that the tortuosity factor increases with increasing nanoplatelet content, an opposite trend was found. Films at 70 wt% of GNPs showed the best protection against moisture uptake. By increasing the filler content, the nanostructure is affected by dry areas and the surface of the film becomes more hydrophilic, promoting moisture absorption.

Nanostructured films with 70 wt% of GNPs represent a promising technology to be employed as barrier coating in the aeronautics field, thanks to the significant reduction of moisture permeation inside composite panels. Compared to existing technologies, these innovative films are lightweight, easily integrated in the manufacturing processes, and are not susceptible to corrosion. In addition, thanks to their low electrical resistivity, they provide additional functionalities as shielding against electrostatic discharges and electromagnetic waves.

Author Contributions: Conceptualization F.C. and A.M.; methodology B.P., G.B. and R.V.; Investigation F.C., G.B., C.C.T. and C.T.; data curation F.C., B.P. and C.T.; writing—original draft preparation F.C., B.P. and R.V.; writing—review and editing A.M., G.G. and M.G.; supervision A.M., M.G. and G.G.; funding acquisition M.G., A.M. and G.G. All authors have read and agreed to the published version of the manuscript.

Funding: This work has been supported by the Research Project AMICO (code ARS01_00758) funded by the Italian Ministry of Education, University and Research.

Institutional Review Board Statement: Not applicable.

Informed Consent Statement: Not applicable.

Data Availability Statement: The data presented in this study are available in the article.

Acknowledgments: The authors would like to thank Nicola Gallo and Giovanni Barletta for their precious advice and discussions.

Conflicts of Interest: The authors declare no conflict of interest.

References

1. Soutis, C. Carbon fiber reinforced plastics in aircraft construction. *Mater. Sci. Eng. A* **2005**, *412*, 171–176. [[CrossRef](#)]
2. Hahn, H.T.; Kim, K.S. Hygroscopic Effects in Aramid Fiber/Epoxy Composite. *J. Eng. Mater. Technol.* **1988**, *110*, 153–157. [[CrossRef](#)]
3. Xiao, G.Z.; Shanahan, M.E.R. Water absorption and desorption in an epoxy resin with degradation. *J. Polym. Sci. Part B Polym. Phys.* **1997**, *35*, 2659–2670. [[CrossRef](#)]
4. Wan, Y.Z.; Wang, Y.L.; Huang, Y.; Luo, H.L.; He, F.; Chen, G.C. Moisture absorption in a three-dimensional braided carbon/Kevlar/epoxy hybrid composite for orthopaedic usage and its influence on mechanical performance. *Compos. Part A Appl. Sci. Manuf.* **2006**, *37*, 1480–1484. [[CrossRef](#)]
5. Eckstein, B.H. Moisture absorption by epoxy laminating resins. *Org. Coat. Plast. Chem.* **1978**, *38*, 503–509.
6. Olmos, D.; López-Morón, R.; González-Benito, J. The nature of the glass fibre surface and its effect in the water absorption of glass fibre/epoxy composites. The use of fluorescence to obtain information at the interface. *Compos. Sci. Technol.* **2006**, *66*, 2758–2768. [[CrossRef](#)]
7. Velmurugan, G.; Natrayan, L. Experimental investigations of moisture diffusion and mechanical properties of interply rearrangement of glass/Kevlar-based hybrid composites under cryogenic environment. *J. Mater. Res. Technol.* **2023**, *23*, 4513–4526. [[CrossRef](#)]
8. Verpoest, I.; Springer, G.S. Moisture Absorption Characteristics of Aramid-Epoxy Composites. *J. Reinf. Plast. Compos.* **1988**, *7*, 2–22. [[CrossRef](#)]
9. Gopalan, R.; Rao, R.M.V.G.K.; Murthy, M.V.V.; Dattaguru, B. Diffusion Studies on Advanced Fibre Hybrid Composites. *J. Reinf. Plast. Compos.* **1986**, *5*, 51–61. [[CrossRef](#)]
10. McKague, E.L., Jr.; Reynolds, J.D.; Halkias, J.E. Swelling and glass transition relations for epoxy matrix material in humid environments. *J. Appl. Polym. Sci.* **1978**, *22*, 1643–1654. [[CrossRef](#)]

11. Mijović, J.; Lin, K. The effect of hygrothermal fatigue on physical/mechanical properties and morphology of neat epoxy resin and graphite/epoxy composite. *J. Appl. Polym. Sci.* **1985**, *30*, 2527–2549. [[CrossRef](#)]
12. Xiao, G.Z.; Shanahan, M.E.R. Swelling of DGEBA/DDA epoxy resin during hygrothermal ageing. *Polymer* **1998**, *39*, 3253–3260. [[CrossRef](#)]
13. Yahaya, R.; Sapuan, S.M.; Jawaid, M.; Leman, Z.; Zainudin, E.S. Water absorption behaviour and impact strength of Kenaf-Kevlar reinforced epoxy hybrid composites. *Adv. Compos. Lett.* **2016**, *25*, 98–102. [[CrossRef](#)]
14. Yeung, K.K.H.; Rao, K.P. Mechanical Properties of Kevlar-49 Fibre Reinforced Thermoplastic Composites. *Polym. Polym. Compos.* **2012**, *20*, 411–424. [[CrossRef](#)]
15. Cise, D.; Lakes, R.S. Moisture ingress in honeycomb core sandwich panels. *J. Mater. Eng. Perform.* **1997**, *6*, 732–736. [[CrossRef](#)]
16. Shafizadeh, J.E.; Seferis, J.C.; Chesmar, E.F.; Frye, B.A.; Geyer, R. Evaluation of the mechanisms of water migration through honeycomb core. *J. Mater. Sci.* **2003**, *38*, 2547–2555. [[CrossRef](#)]
17. Glass, D.E.; Raman, V.V.; Venkat, V.S.; Sankaran, S.N. *Honeycomb Core Permeability under Mechanical Loads*; No. NASA/CR-97-206263; NASA: Washington, DC, USA, 1997.
18. Choi, H.S.; Jang, Y.H. Bondline strength evaluation of cocure/precured honeycomb sandwich structures under aircraft hygro and repair environments. *Compos. Part A Appl. Sci. Manuf.* **2010**, *41*, 1138–1147. [[CrossRef](#)]
19. Sturgeon, A.; Dunn, B.; Celotto, S.; O'Neill, W. Cold sprayed coatings for polymer composite substrate. *ESA SP* **2006**, *616*, 1–5.
20. Edrisy, A.; Perry, T.; Cheng, Y.T.; Alpas, A.T. The effect of humidity on the sliding wear of plasma transfer wire arc thermal sprayed low carbon steel coatings. *Surf. Coat. Technol.* **2001**, *146–147*, 571–577. [[CrossRef](#)]
21. Boningari, T.; Inturi, S.N.R.; Suidan, M.; Smirniotis, P.G. Novel one-step synthesis of sulfur doped-TiO₂ by flame spray pyrolysis for visible light photocatalytic degradation of acetaldehyde. *Chem. Eng. J.* **2018**, *339*, 249–258. [[CrossRef](#)]
22. Steven, M.D.; Hotchkiss, J.H. Comparison of flat film to total package water vapour transmission rates for several commercial food wraps. *Packag. Technol. Sci.* **2002**, *15*, 17–27. [[CrossRef](#)]
23. Zhao, O.; Ding, Y.; Pan, Z.; Rolston, N.; Zhang, J.; Dauskardt, R.H. Open-Air Plasma-Deposited Multilayer Thin-Film Moisture Barriers. *ACS Appl. Mater. Interfaces* **2020**, *12*, 26405–26412. [[CrossRef](#)]
24. Hirvikorpi, T.; Vähä-Nissi, M.; Mustonen, T.; Iiskola, E.; Karppinen, M. Atomic layer deposited aluminum oxide barrier coatings for packaging materials. *Thin Solid Film.* **2010**, *518*, 2654–2658. [[CrossRef](#)]
25. Gaztelumendi, I.; Chapartegui, M.; Seddon, R.; Flórez, S.; Pons, F.; Cinquin, J. Enhancement of electrical conductivity of composite structures by integration of carbon nanotubes via bulk resin and/or buckypaper films. *Compos. Part B Eng.* **2017**, *122*, 31–40. [[CrossRef](#)]
26. Kececi, E.; Asmatulu, R. Effects of moisture ingresses on mechanical properties of honeycomb-structured fiber composites for aerospace applications. *Int. J. Adv. Manuf. Technol.* **2017**, *88*, 459–470. [[CrossRef](#)]
27. Kececi, E.; Asmatulu, R. Effects of moisture ingress on polymeric laminate composites and its prevention via highly robust barrier films. *Int. J. Adv. Manuf. Technol.* **2014**, *73*, 1657–1664. [[CrossRef](#)]
28. Ebnesajjad, S. Polyvinyl Fluoride: The First Durable Replacement for Paint. In *Introduction to Fluoropolymers*; Elsevier: Amsterdam, The Netherlands, 2013; pp. 53–61.
29. Cui, Y.; Kundalwal, S.I.; Kumar, S. Gas barrier performance of graphene/polymer nanocomposites. *Carbon N. Y.* **2016**, *98*, 313–333. [[CrossRef](#)]
30. Cilento, F.; Leone, C.; Genna, S.; Giordano, M.; Martone, A. Graphene NanoPlatelet-based coating as thermal protection from high-power radiative fluxes. *Compos. Struct.* **2023**, *319*, 117157. [[CrossRef](#)]
31. Wu, H.; Drzal, L.T. Graphene nanoplatelet paper as a light-weight composite with excellent electrical and thermal conductivity and good gas barrier properties. *Carbon N. Y.* **2012**, *50*, 1135–1145. [[CrossRef](#)]
32. Li, X.; Manasrah, A.; Al-ostaz, A.; Alkhateb, H.; Lincoln, D.; Rushing, G.; Cheng, A.H. Preparation and Characterization of High Content Graphene Nanoplatelet-Polyetherimide Paper. *J. Nanosci. Nanoeng.* **2015**, *1*, 252–258.
33. Palen, B.; Iverson, E.T.; Rabaey, M.G.; Kulatilaka, S.; Grunlan, J.C. Graphene oxide nanobrick wall for gas barrier and fire protection of polystyrene. *J. Mater. Sci.* **2023**, *58*, 7594–7601. [[CrossRef](#)]
34. Yin, C.; Du, X.; Ding, Z.; Zeng, Q.; Li, X.; He, C.; Xiong, B.; Li, J.; Zhou, Y. Gas permeation and microstructure of reduced graphene oxide/polyethyleneimine multilayer films created via recast and layer-by-layer deposition processes. *RSC Adv.* **2022**, *12*, 6561–6572. [[CrossRef](#)]
35. Fu, Y.; Hansson, J.; Liu, Y.; Chen, S.; Zehri, A.; Samani, M.K.; Wang, N.; Ni, Y.; Zhang, Y.; Zhang, Z.-B.; et al. Graphene related materials for thermal management. *2D Mater.* **2020**, *7*, 012001. [[CrossRef](#)]
36. Chen, S.; Wang, Q.; Zhang, M.; Huang, R.; Huang, Y.; Tang, J.; Liu, J. Scalable production of thick graphene film for next generation thermal management application. *Carbon N. Y.* **2020**, *167*, 270–277. [[CrossRef](#)]
37. Lahbacha, K.; Sibilica, S.; Trezza, G.; Giovinco, G.; Bertocchi, F.; Chiodini, S.; Cristiano, F.; Maffucci, A. Electro-Thermal Parameters of Graphene Nano-Platelets Films for De-Icing Applications. *Aerospace* **2022**, *9*, 107. [[CrossRef](#)]
38. Vertuccio, L.; Foglia, F.; Pantani, R.; Romero-Sánchez, M.D.; Calderón, B.; Guadagno, L. Carbon nanotubes and expanded graphite based bulk nanocomposites for de-icing applications. *Compos. Part B Eng.* **2021**, *207*, 108583. [[CrossRef](#)]
39. Palmieri, B.; Cilento, F.; Siviello, C.; Bertocchi, F.; Giordano, M.; Martone, A. Mitigation of Heat Propagation in a Battery Pack by Interstitial Graphite Nanoplatelet Layer: Coupled Electrochemical-Heat Transfer Model. *J. Compos. Sci.* **2022**, *6*, 296. [[CrossRef](#)]

40. Huang, P.; Li, Y.; Yang, G.; Li, Z.-X.; Li, Y.-Q.; Hu, N.; Fu, S.-Y.; Novoselov, K.S. Graphene film for thermal management: A review. *Nano Mater. Sci.* **2021**, *3*, 1–16. [[CrossRef](#)]
41. Chen, Y.; Li, J.; Li, T.; Zhang, L.; Meng, F. Recent advances in graphene-based films for electromagnetic interference shielding: Review and future prospects. *Carbon N. Y.* **2021**, *180*, 163–184. [[CrossRef](#)]
42. Wei, Q.; Pei, S.; Qian, X.; Liu, H.; Liu, Z.; Zhang, W.; Zhou, T.; Zhang, Z.; Zhang, X.; Cheng, H.; et al. Superhigh Electromagnetic Interference Shielding of Ultrathin Aligned Pristine Graphene Nanosheets Film. *Adv. Mater.* **2020**, *32*, 1907411. [[CrossRef](#)]
43. Kumar, S.S.A.; Uddin, M.N.; Rahman, M.M.; Asmatulu, R. Introducing graphene thin films into carbon fiber composite structures for lightning strike protection. *Polym. Compos.* **2019**, *40*, E517–E525. [[CrossRef](#)]
44. Zhu, Y.; Ming, Y.; Sun, J.; Li, S.; Li, S.; Xiao, H.; Wang, B.; Duan, Y. Joule heating synthesis of carbon fiber/graphene 3D crosslinked structure for lightning strike protection and electromagnetic interference in aerospace composites. *Chem. Eng. J.* **2023**, *474*, 145583. [[CrossRef](#)]
45. Wang, B.; Duan, Y.; Xin, Z.; Yao, X.; Abliz, D.; Ziegmann, G. Fabrication of an enriched graphene surface protection of carbon fiber/epoxy composites for lightning strike via a percolating-assisted resin film infusion method. *Compos. Sci. Technol.* **2018**, *158*, 51–60. [[CrossRef](#)]
46. Cilento, F.; Martone, A.; Pastore Carbone, M.G.; Galiotis, C.; Giordano, M. thermallike GNP/Epoxy composites: Reinforcement efficiency vis-à-vis graphene content. *Compos. Sci. Technol.* **2021**, *211*, 108873. [[CrossRef](#)]
47. *ASTM-D5229*; Standard Test Method for Moisture Absorption Properties and Equilibrium Conditioning of Polymer Matrix Composite Materials. ASTM: West Conshohocken, PA, USA, 2020.
48. Breitenstein, O.; Altmann, F. *Application of Lock-in Thermography to Failure Analysis in Integrated Circuits*; Microtherm: Halle, Germany, 2011; pp. 1–6.
49. Tyler, W.W.; Wilson, A.C., Jr. Thermal conductivity, electrical resistivity, and thermoelectric power of graphite. *Phys. Rev.* **1953**, *89*, 870. [[CrossRef](#)]
50. Carter, S. Electrostatic Discharge (ESD) Properties of Plastic Packaging: Terminology. *Stand. Meas. Tek Pak Tech. Bull.* **1985**, *101*, 1–5.
51. Cilento, F.; Curcio, C.; Martone, A.; Liseno, A.; Capozzoli, A.; Giordano, M. Effect of Graphite Nanoplatelets Content and Distribution on the Electromagnetic Shielding Attenuation Mechanisms in 2D Nanocomposites. *J. Compos. Sci.* **2022**, *6*, 257. [[CrossRef](#)]
52. van Es, M.A. Polymer-Clay Nanocomposites: The Importance of Particle Dimensions. Ph.D. Thesis, Delft University of Technology, Delft, The Netherlands, 2001; p. 252.
53. Aronhime, M.T.; Neumann, S.; Marom, G. The anisotropic diffusion of water in Kevlar-epoxy composites. *J. Mater. Sci.* **1987**, *22*, 2435–2446. [[CrossRef](#)]
54. Li, J.; Wang, S.; Lai, L.; Liu, P.; Wu, H.; Xu, J.; Severtson, S.J.; Wang, W.-J. Synergistic enhancement of gas barrier and aging resistance for biodegradable films with aligned graphene nanosheets. *Carbon N. Y.* **2021**, *172*, 31–40. [[CrossRef](#)]
55. Nielsen, L.E. Models for the Permeability of Filled Polymer Systems. *J. Macromol. Sci. Part A-Chem.* **1967**, *5*, 37–41. [[CrossRef](#)]
56. Zeng, Q.; Yin, C.; Li, X.; He, C. Linear relationship between lateral size of reduced graphene oxide (RGO) and water vapor barrier property in RGO/PEI composite membrane. *J. Memb. Sci.* **2023**, *684*, 121876. [[CrossRef](#)]
57. Cilento, F.; Martone, A.; Cristiano, F.; Fina, A.; Giordano, M. Effect of Matrix Content on Mechanical and Thermal Properties of High Graphene Content Composites. *MATEC Web Conf.* **2019**, *303*, 01002. [[CrossRef](#)]
58. Cilento, F.; Martone, A.; Giordano, M. Insights on Shear Transfer Efficiency in “Brick-and-Mortar” Composites Made of 2D Carbon Nanoparticles. *Nanomaterials* **2022**, *12*, 1359. [[CrossRef](#)] [[PubMed](#)]
59. Miao, A.; Wei, M.; Xu, F.; Wang, Y. Influence of membrane hydrophilicity on water permeability: An experimental study bridging simulations. *J. Memb. Sci.* **2020**, *604*, 118087. [[CrossRef](#)]
60. Pandit, S.; Gaska, K.; Mokkapatil, V.R.S.S.; Celauro, E.; Derouiche, A.; Forsberg, S.; Svensson, M.; Kádár, R.; Mijakovic, I. Precontrolled Alignment of Graphite Nanoplatelets in Polymeric Composites Prevents Bacterial Attachment. *Small* **2020**, *16*, 1904756. [[CrossRef](#)]
61. Czerwinski, F. Thermal Stability of Aluminum Alloys. *Materials* **2020**, *13*, 3441. [[CrossRef](#)]

Disclaimer/Publisher’s Note: The statements, opinions and data contained in all publications are solely those of the individual author(s) and contributor(s) and not of MDPI and/or the editor(s). MDPI and/or the editor(s) disclaim responsibility for any injury to people or property resulting from any ideas, methods, instructions or products referred to in the content.